An assessment of the local sea-level budget and the present trajectory of sea-level rise at tide-gauge locations

Thomas Frederikse (thomas.frederikse@jpl.nasa.gov)
Jet Propulsion Laboratory, California Institute of Technology https://orcid.org/0000-0002-5024-0163
Benjamin Hamlington
Jet Propulsion Laboratory https://orcid.org/0000-0002-5731-9966
Thomas Harvey
Divirod Inc. https://orcid.org/0000-0002-7458-1990
William Sweet
National Oceanic and Atmospheric Administration
Ian Fenty
Jet Propulsion Laboratory, California Institute of Technology https://orcid.org/0000-0001-6662-6346
Ou Wang
Jet Propulsion Lab
Ichiro Fukumori
Jet Propulsion Laboratory, California Institute of Technology

Article

Keywords:

Posted Date: May 19th, 2022

DOI: https://doi.org/10.21203/rs.3.rs-1623226/v1

An assessment of the local sea-level budget and the present trajectory of sea-level rise at tide-gauge locations

Thomas Frederikse[1,2*], Ben Hamlington[1], Cam Harvey[1], William Sweet[3], Ian Fenty[1], Ou Wang[1], and Ichiro Fukumori[1]

[1]Jet Propulsion Laboratory, California Institute of Technology
[2]University of California, Los Angeles
[3]NOAA National Ocean Service
[*]thomas.frederikse@jpl.nasa.gov

ABSTRACT

Local sea-level changes deviate from the global mean and unforced variability often masks sea-level changes driven by greenhouse forcing. Both cause difficulties when local observations are compared to projections. We present two analyses of local sea level aiming at improving understanding local causes of sea-level rise and variability. First, we analyse local sea-level budgets at 557 tide-gauge locations from 1993-2019. On average, the sum of contributing processes explains 49% of the observed inter-annual variance. Sterodynamic processes explain most of the variability. The average observed trend is 2.6 mm yr^{-1} with contributors summing up to 2.7 mm yr^{-1}. Secondly, we extrapolate the current trajectory of sea-level rise and estimate how unforced variability can mask or exaggerate future long-term sea-level changes. Unforced variability can cause sea-level changes up to multiple decimeters on 30-year time scales, and the differences between projections and the trajectory are thus generally not significant.

Introduction

Global sea level has been rising over the past decades with an accelerating rate[1], but local sea levels often deviate from this global mean[2]. Because local sea level is generally the quantity of interest for coastal planners[3], understanding the causes and future of local sea-level rise is of high importance. To make accurate projections of local sea level, a complete picture of the underlying local processes is needed. Furthermore, unforced variability also cause sea-level changes, which can hide or exaggerate the underlying long-term sea-level rise due to greenhouse forcing[4]. With unforced variability, we refer to sea-level variations, either global or local, that are not caused by greenhouse forcing[5]. In this paper, we present a set of tools that can help with these open questions. We present an analysis of the local sea-level budget at 557 tide-gauge locations, which gives insight into local processes that cause sea-level changes, and can tell whether these known processes explain the observations. Secondly, we compute the present-day long-term trajectory of sea-level rise and analyse the extent of which unforced variability can hide or exaggerate longer-term sea-level changes in the coming few decades.

The causes of global-mean sea level change have been reasonably understood[6], but for local sea level, the driving processes behind the observed variability and trends are often still uncertain[7]. Among others, reasons for this uncertainty are local processes that can vary over small spatial scales that are difficult to measure and model, such as local ocean dynamic effects and local vertical land motion[8]. Comparing the observed sea-level trends and variability to the sum of estimates of the known underlying processes can shed light on the nature of these sea-level changes. This budget approach has been used for example to estimate how open-ocean variability affects coastal sea levels[9] and to infer visco-elastic properties of the solid Earth underneath the U.S. East Coast[10]. Because of these hard-to-quantify processes a comprehensive explanation of observed sea-level trends and variability over the last few decades has only been achieved for a limited set of locations, such as the European and US Atlantic coasts[10–12]. Over the last few years, significant progress has been made on this issue: the longer-term observed trends can now be explained at most tide-gauge locations, albeit with substantial margins of uncertainty[2,13]. Finally, reasonable agreement has been found between regional sea-level projections from the IPCC AR5 report[14] and long-term trends in observations[15]. However, a complete assessment of the local sea-level budget that assesses both trends and inter-annual variability is still missing to the best of our knowledge.

Another challenge that is related to the aforementioned budget problem, is to separate inter-annual, decadal, and multi-

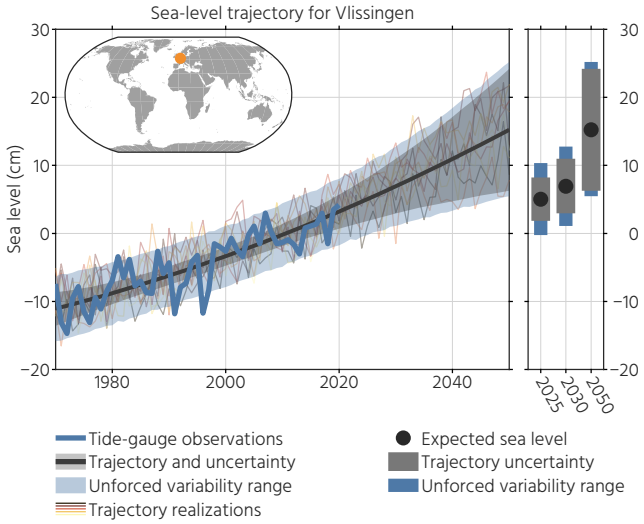

Figure 1. An example trajectory computation for the Vlissingen tide gauge. The blue line shows observed annual-mean sea level. The black line is the median trajectory, and the shade is the 5th-95th percentile due to uncertainties in the trajectory. The blue shade shows the combined uncertainty due to trajectory uncertainty and unforced variability. The thin colored lines depict a few random realizations of the trajectory and unforced variability. The bar graphs on the right show the median trajectory extrapolation for a specific year, with respect to mean sea level during 2001-2020, as well as the trajectory uncertainty and unforced variability range.

decadal variability that is not linked to climatic forcing, from long-term forced sea-level changes and other stable processes, like glacial isostatic adjustment (GIA). This unforced variability can suppress or add to the trends and acceleration in observed sea levels[4], even on centennial time scales[16]. Due to this unforced variability, future local sea-level trends and accelerations can deviate from projected sea levels. By quantifying this variability and the long-term trend and acceleration, we can assess a likely range of future sea-level change and determine whether any deviation from sea-level projections is significant or can still be attributed to unforced variability.

Here, we assess both issues: we estimate the sea-level budget at 557 tide-gauge locations and determine whether the estimated sum of contributors can explain the observed trend and inter-annual variability during 1993-2019. This time frame has been chosen because it coincides with the period for which the ECCO framework (see Methods) provides estimates of sterodynamic sea level. This work is an extension of sea-level budget analysis from ref.[12], which analysed the contributors to the observed sea-level trends along the U.S. coastlines. Here, we expand this analysis to a global set of coastal locations and analyse the annual time series to determine the extent of which we understand inter-annual variability. Furthermore, we present an estimate of the present-day trajectories of local sea level. With trajectory, we mean the trend and acceleration in observed sea level since 1970. We estimate the trajectory at each of the 557 tide-gauge locations and determine the variability around this trajectory. We extrapolate the trajectory and generate random realizations of the variability to estimate the likely range of future sea-level change. These extrapolated trajectories can serve as an estimate of how sea level will change if it keeps following the same pathway as over the last few decades. We compare these trajectories with the projections of local sea level from the IPCC AR6 WG1 report[17,18] to determine whether the projected sea-level changes in the coming decades are in line with the extrapolation of the present-day trajectories, or whether coastal communities can expect a deviation from the current trajectory. The presence of unforced sea-level variability has two consequences for estimating the trajectory and its extrapolation: First, the unforced variability affects the estimated trend and acceleration, which causes uncertainty in the extrapolated trajectory, and secondly, future variability will lead to departures from this trajectory. Together, these effects will create an envelope of possible sea-level changes about the estimated trajectory. We account for both processes, and assess each effect separately. Figure 1 depicts an example of this trajectory, and how unforced variability affects the estimated trajectory and can lead to deviations from the trajectory in the future.

Results

The sea-level budget

Figure 2 shows the sea-level budget for four locations for which the sum of contributors explains the observed trends and variability well. For each of the four locations, the year-to-year variability due to vertical land motion and GIA is zero, because

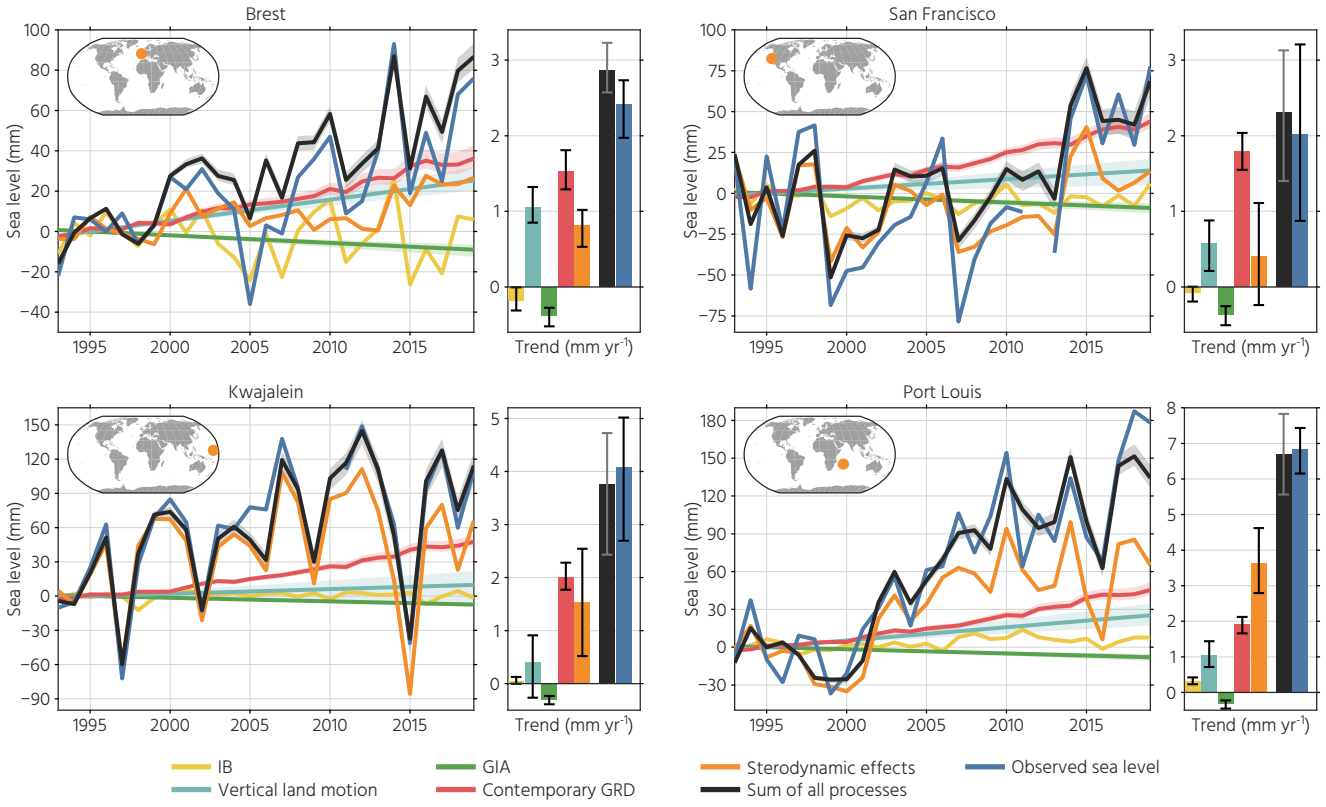

Figure 2. Example sea-level budget time series and trends. Each line shows annual-mean sea level, and each bar shows the linear trend over 1993-2019. For processes where we have an estimate of the uncertainty (GIA, contemporary GRD, and VLM) the shading shows the 5-95% confidence interval. The black lines in the bar graphs also show the 5-95% confidence intervals.

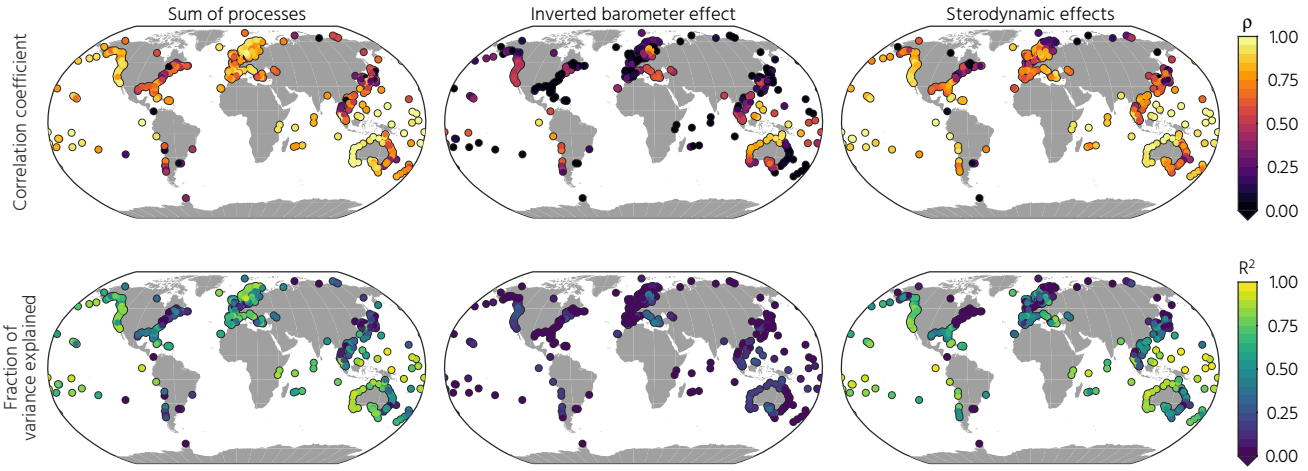

Figure 3. Statistics of the inter-annual variability after de-trending all the time series. Top panels show the correlation coefficient, and the bottom panels show the explained fraction of variance (R^2).

we model them as a linear trend. The inter-annual variability due to barystatic sea level and associated FGSLcontemporary geoid, rotation, and deformation (GRD) effects is also small. For all four stations, except Brest, ocean dynamics are the dominant cause of inter-annual variability. This behaviour is in line with what is seen on a global scale from altimetry, where ocean dynamic processes and associated teleconnection patterns explain the vast majority of inter-annual variability[19,20]. The causes of this variability vary from place to place, and can be associated with various phenomena. In the example stations shown here, the anti-correlated patterns visible for San Francisco and Kwajalein, which are in the East- and West-Pacific oceans, are related to a large-scale mode of sea-level variability linked to ENSO and the Pacific Decadal Oscillation[21]. For Brest, interannual sea-level variability has been linked to wind-driven coastally-trapped waves that cause spatially-coherent sea-level fluctuations along the Northeast Atlantic coasts[22].

In contrast to the other three stations in Figure 2, the inverted barometer effect explains a substantial fraction of the observed interannual variability in Brest. For most other stations, the impact of the inverted barometer effect on annual sea level is typically small: Figure 3 shows that the sum of contributors typically explain a substantial part of the variability: the median fraction of explained variance (R^2) of de-trended sea-level observations is 49%. Sterodynamic effects as simulated with ECCO have a median R^2 of 34%, while the inverse barometer effect has a median R^2 of just 1 %. The fraction of explained variance of observed sea-level variability in Figure 3 varies considerably: islands and eastern ocean boundaries show a higher correlation and fraction of explained variance than western ocean boundaries, which might be explained by the strongly eddying western boundary currents, which the ECCO model resolution is too coarse to explicitly resolve for.

While the inter-annual variability after de-trending is dominated by sterodynamic effects and for a few locations by the inverse barometer effect, the causes of the linear trend over 1993-2019 are more diverse. The example stations in Figure 2 show that all processes together explain the observed trend, with no single process standing out as the most influential factor. Vertical land motion and sterodynamic effects vary the most between these stations, while GIA and contemporary GRD effects are relatively similar among stations. This is a consequence of how budget has been constructed, as explained in the Methods section: the GIA and contemporary GRD effects only represent geocentric sea level (GSL). Because GSL does not include sea-level changes induced by solid-Earth deformation, which determines most of the spatial variations in GRD relative sea level (RSL) patterns, they only have limited spatial variations. This limited spread is visible in Figure 4: most spatial variations in the sum of contributing processes can be tied to vertical land motion and sterodynamic processes.

Vertical land motion is responsible for the low trends in Northern Europe and Alaska. The uplift in this region is tied to GIA[23] and mass loss of the Alaskan glaciers[24]. The residual subsidence in Australia has been observed in other studies as well, but the causes of it are still unknown[25]. The residual subsidence along the US East and Gulf coasts has been linked to both GIA and local processes, such as sediment compaction and groundwater extraction[26,27]. The spatial variability in the ocean dynamic trends also reflect some well-known patterns, such as the low trends in large parts of the Pacific[21], and high trends along the US Atlantic and Gulf coasts[12]. Often, the physical processes and the attribution of these regional sea-level trends to either unforced variability or a forced response to greenhouse gas forcings are not yet fully understood. For example, the causes and spatial patterns of dynamic sea level along the US East Coasts are still being discussed[28,29].

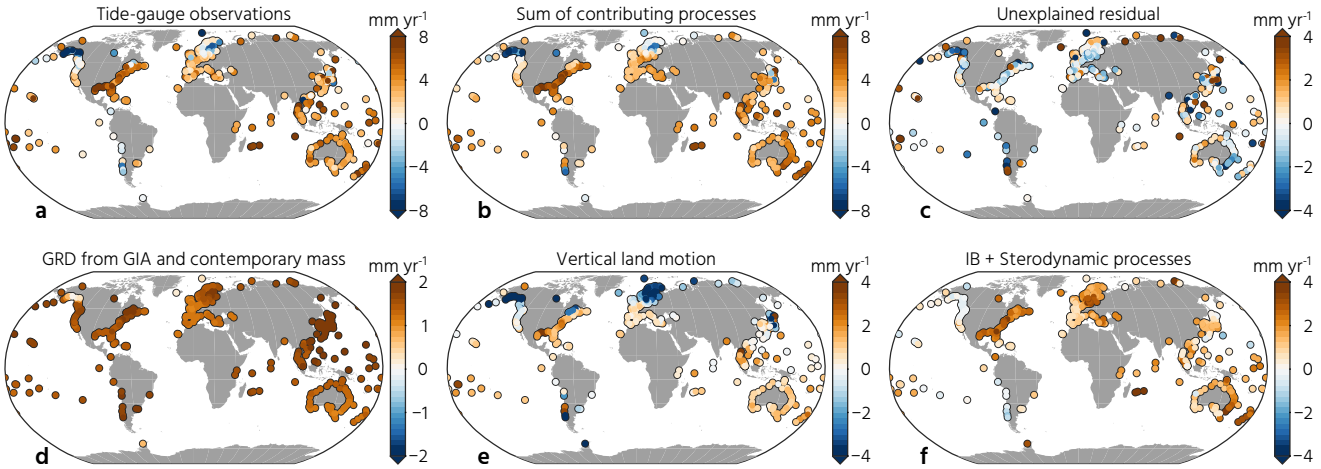

Figure 4. Linear trends (1993-2019) in observed sea level (panel a), the budget components (panels d-f), their sum (panel b), and the unexplained residual trend (panel c). The trend in panel d shows the sum of GIA and contemporary GRD, and panel f shows the sum of sterodynamic sea-level variations and the IB effect. Note that the color scale differs for each row and column.

Trajectories and projections

Figure 5 shows the median sea-level trajectory extrapolated to 2025, 2030 and 2050, as well as the spread (defined here as the difference between the 5th and 95th percentile) due to uncertainties in the trajectory and due to unforced variability. Akin to the observed trends over 1993-2019 (Figure 4), the extrapolated trajectories show a substantial spread, with some regional patterns emerging. Along the US East and Gulf coasts and the Western Pacific, the mean trajectory points at a large sea-level rise, while it points at a limited rise for Northern Europe and Alaska.

The uncertainties in the trajectory are substantial: in 2025, the spread due to uncertainties in the extrapolated trajectory (the grey area in Figure 1) is still limited to a few cm for most places. However, inter-annual variability results in a much higher total spread in expected sea level (the blue area in Figure 1). That means that for many locations, a sea-level drop in 2025 relative to the 2001-2020 mean is within the expected range of unforced variability. For 2030 and 2050, the trajectory uncertainty becomes the dominant cause of the total spread. Annual-mean sea level in 2050 could still be below the 2001-2020 mean within the 5-95th percentile for 198 out of 557 locations. The opposite is also possible: annual-mean sea levels of multiple decimeters above the mean trajectories in 2050 do not point at a significant deviation from these trajectories. This again points out that unforced variability can mask out underlying sea-level rise for multiple decades at many places.

To determine whether the present-day trajectory is representative of longer-term sea-level changes as projected from physical models, we compared the extrapolated trajectories with the projections from the IPCC AR6 report. Figure 6 shows whether the extrapolated trajectories are within the range of the AR6 projections in 2050, and which SSP scenario is closest to the trajectory in 2050. This comparison can inform coastal communities on whether the observed sea-level trajectory is likely to change to meet specific projections. For example, for many European locations, the trajectory matches the SSP 1.19 scenario, which suggests that when emissions and greenhouse gas concentrations will follow a higher pathway, these locations can expect a larger acceleration in future sea level than currently observed. The opposite happens along most United States coastlines, where the present-day trajectory most closely aligns to the high-end SSP 5.85 scenario.

For 141 out of 557 stations, the trajectory diverges significantly from all scenarios in 2050 (Diamonds and squares in Figure 6). Most of these stations are in regions where local processes cause non-linear vertical land motion, which is not included in the AR6 projections[18]. For example, stations along the South-eastern Pacific coast and in Japan are affected by tectonic activity. Stations in the Arctic region close to glaciers that show accelerating mass loss will be affected by large uplift signals[24]. For some other stations, it might point at large multi-decadal variability patterns that are not well represented by a first-order autoregressive process.

The results from Figure 6 might trigger the question whether the observations and trajectory can be used to assess the likelihood of specific sea-level scenarios and to assess the quality of these projections. As shown in Figure 7, the median trajectories often do not align with the scenarios, but most scenarios fall within the uncertainty range of the trajectory. For Vlissingen (Figure 7a), the scenarios show an acceleration that is not reproduced by the median trajectory, but due to the uncertainties in that trajectory, the actual presence of a long-term acceleration hidden underneath unforced variability can not be ruled out. The opposite situation can be seen in Galveston (Figure 7b) and Montevideo (Figure 7c): here the median trajectory

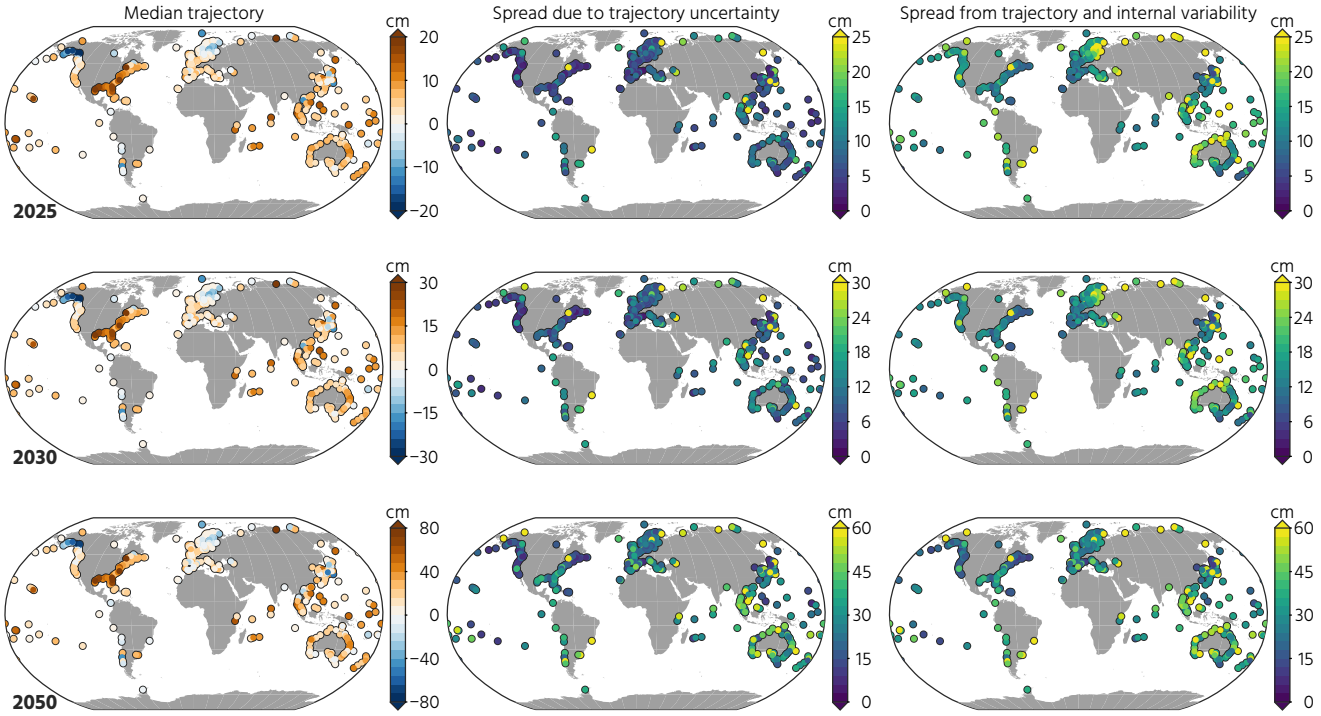

Figure 5. Extrapolated trajectories and their uncertainties relative to mean sea level over 2001-2020. The left column shows the median. The middle column shows the spread, defined as the 95th percentile minus the 5th percentile, due to the uncertainties in the trajectory estimation. The right column shows the spread due to unforced variability and trajectory uncertainty. Note that the color scale differs for each row and column.

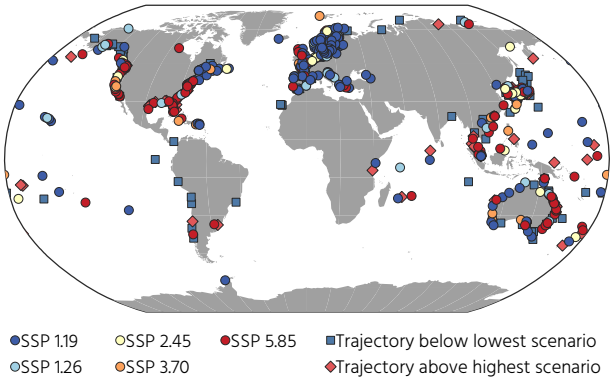

Figure 6. Comparison of extrapolated trajectories and sea-level projections from the IPCC AR6 under various SSP scenarios for the year 2050. A blue square denotes a location at which the trajectory is significantly (90% C.I.) below the lowest scenario in 2050. A red diamond denotes a location where the trajectory gives a significantly (90% C.I.) higher sea level than the highest scenario. The color of the circles shows the scenario that is closest to the extrapolated scenario in 2050.

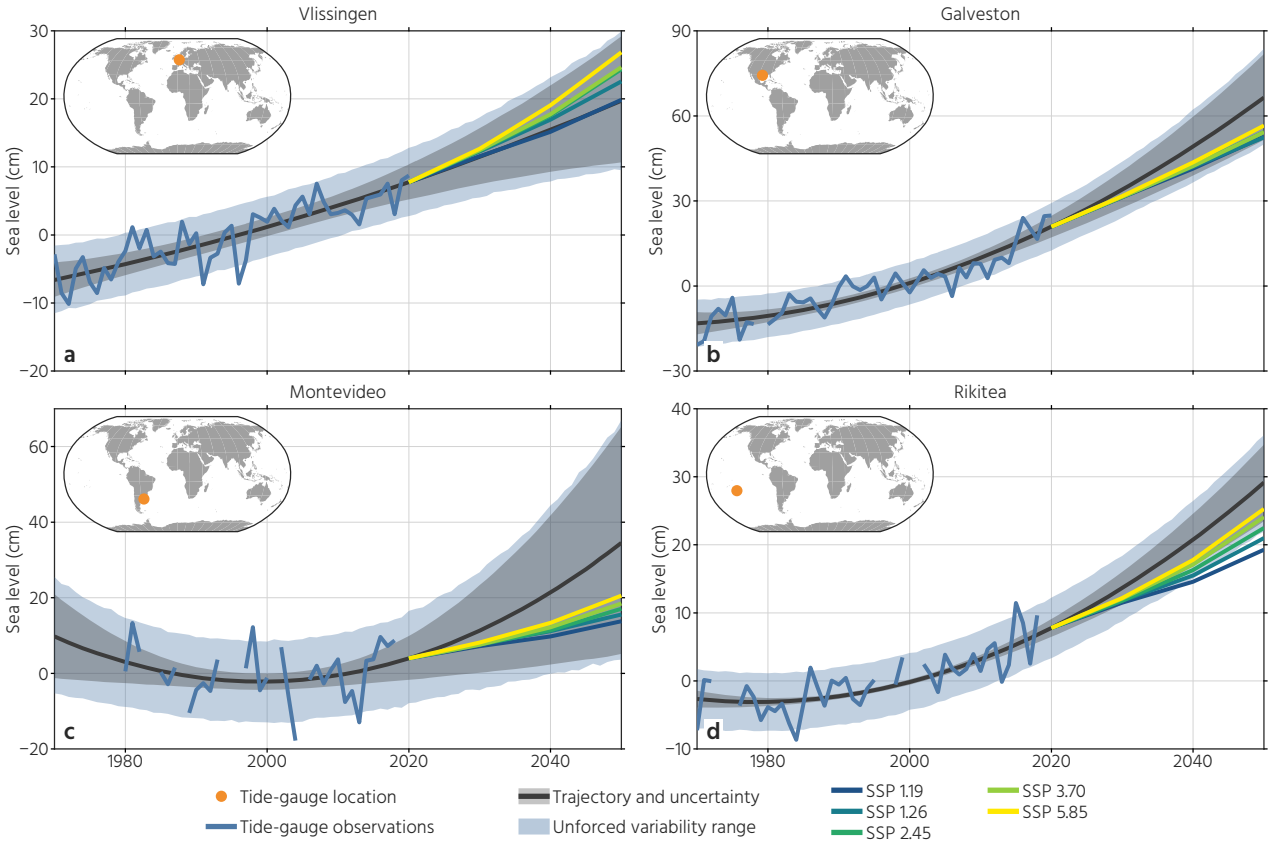

Figure 7. Trajectories compared to AR6 sea-level projections for four example locations. The orange dot in the top left corner of each panel shows the tide-gauge location. Note that the y-axis range differs among the panels.

shows a stronger acceleration and higher sea level than all the AR6 scenarios. However, uncertainties again show that the present trajectory does not significantly deviate from the scenarios. For Montevideo, the large interannual variability combined with gaps in the tide-gauge record cause a large range of uncertainty in the record. In Rikitea (Figure 7d), the median lower-end scenarios fall outside the trajectory range. This might be caused by multi-decadal variability on time scales longer than the 50-year records used here that leaks into the estimated trend and acceleration. Furthermore, the projections themselves also have an uncertainty range, which is not shown in Figure 7, and in the case of Rikitea, no scenario deviates significantly from the trajectory when taking both trajectory and scenario uncertainty into account.

Discussion

In this study we have analysed two subjects. First, we estimated the local sea-level budget at 557 tide gauges during 1993-2019. Secondly, we computed the present-day trajectory from observations and extrapolated this trajectory into the future.

We find that recent estimates of the contributing factors of sea level explain a large fraction of the observed trends and inter-annual variability over 1993-2019. This conclusion is in line with the recent study from[13], which also reports closure of the sea-level budget, albeit over a different period (1958-2015 versus 1993-2019 here). Our sum of contributors has a mean trend of 2.7 mm yr^{-1} versus 2.6 mm yr^{-1} for the tide-gauge observations. The sum of contributors explains 49% of the observed variance (Figure 3). Sterodynamic sea-level variations are by far the largest contributor to interannual variability, with a small fraction explained by the inverse barometer effect. In contrast, the observed linear trend is often explained by a combination of different processes, and is not dominated by one single process (Figure 4).

Despite the progress in understanding the local sea-level budget, many knowledge gaps, unexplained residual trends, and residual variability remain. Its causes differ from place to place and are often not fully understood. Among possible candidates are vertical land motion, whose estimate is often hindered due to a lack of observations and the lack of a geodetic tie between the tide gauge and the GPS receiver[30]. Understanding how ocean dynamics affect coastal sea level also remains a knowledge gap: for many coastal locations, the sum of contributors only explains a limited fraction of the total inter-annual variance (Figure 3), which suggests that a large fraction of sterodynamic sea-level variability in observed sea level remains un-explained by the budget.

The extrapolated trajectory and the likely range of future sea-level change under this extrapolated trajectory again highlight that unforced variability can hide or exaggerate the underlying long-term sea-level changes for the coming decades. The comparison of the extrapolated trajectory to the IPCC AR6 projections in Figure 6 shows that most trajectories are either tracking the lowest (SSP1.19) or highest (SSP5.85) scenario. Given that both scenarios require either a radical decarbonization or have emissions way above international agreements, a scenario in the middle has a more likely outcome[31]. That means, it is not unlikely for these locations to see a shift of the present trajectory: either a higher acceleration for the stations that track the SSP1.19 scenario or are even below that, and a slowdown for the stations that track SSP5.85. However, due to the large range of unforced variability, a shift of the trajectory can be difficult, if not impossible, to distinguish from this variability, as can be seen from Figure 7. For most of the 141 stations where the trajectory significantly deviates from any scenario, local processes that are not modelled in the scenarios or act on very small spatial scales, such as tectonic activity or complex land motion patterns close to melting glaciers, likely contribute to this mismatch.

The trajectory uncertainties are generally too large to infer issues with the sea-level scenarios: Figure 7 shows some examples of stations where the mean trajectory diverges from the mean scenarios, but the scenarios fall within uncertainties in the trajectories. Therefore, directly comparing observations to trajectories without taking the full uncertainties in the observations into account could lead to false conclusions about issues with the scenarios.

To assist coastal planners, local communities, and other interested people, with an assessment of local sea level, we generated a single-page overview for each tide-gauge station that shows the local tide-gauge observations, the components of the sea-level budget, and the trajectory and projections for each tide-gauge location. We also provide a range of sea level in 2030 and 2050 under the trajectories and for the SSP scenarios.

Methods

In this paper, we use two distinct concepts: the-sea level budget, where we compare time series of observed sea level to estimates of the underlying processes, and the present-day trajectory of sea level, which we extrapolate and compare to physics-based sea-level projections. We assess the local sea-level budget over 1993-2019 and compute the trajectory over 1970-2050. In this section, we first discuss the methods behind the sea-level budget analysis, and then we show how we derive the sea-level trajectories.

The sea-level budget

For the sea-level budget, we compare tide-gauge observations η_{TG} to the sum of underlying processes η_{sum}. Here we consider the following processes: η_{GIA} are sea-level variations due to glacial isostatic adjustment. η_{bGRD} are sea-level variations due

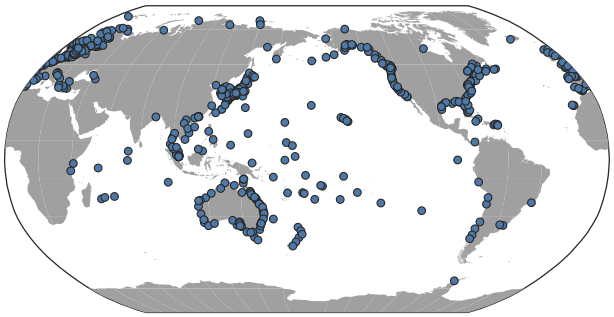

Figure 8. Locations of the 557 tide-gauge stations used in this study

to barystatic processes (i.e. global-mean sea-level changes due to water added and/or removed from the global oceans) and the local sea-level changes due to geoid, rotation, and deformation (GRD) effects induced by the barystatic changes[32]. η_{IB} is the inverse barometer (IB) effect, which is the static response of sea level to atmospheric pressure variations[33]. η_{VLM} are sea-level variations due to vertical land motions: tide gauges measure relative sea level (RSL), which is sea level relative to the solid Earth. This implies that when the solid Earth moves vertically, the tide gauge will register this motion as a sea-level change in the opposite direction. η_{STD} are sea-level variations due to sterodynamic processes: the combined effects of global thermosteric expansion and local ocean dynamics.

$$\eta_{sum,TG} = \eta_{GIA} + \eta_{bGRD} + \eta_{STD} + \eta_{IB} + \eta_{VLM} \tag{1}$$

The choice to include η_{VLM} in Equation 1 has the consequence that VLM induced by GIA and contemporary GRD effects are included in the η_{VLM} term and we should use the GSL effects due to GIA and contemporary GRD effects in this equation. For each of these terms, and for the observations, we compute annual-mean values.

To compute trends, we assume that all time series exhibit first-order autoregressive noise. We estimate the spectral properties of the noise and generate 100 random realizations of the noise using the Hector software[34]. We then add this noise to the time series and estimate the trend through each ensemble member, which provides the mean and standard error of the trends and accelerations. For η_{GIA} and η_{VLM}, for which we only have an estimate of the linear trend, we use the trends directly without the aforementioned procedure.

Sea-level observations and atmospheric data

For the budget and trajectory analysis, we use annual-mean tide-gauge observations from the Permanent Service for Mean Sea Level[35,36] over 1970-2020. We have selected all stations that have more than 20 years of data since 1993. We disregarded all years that are flagged for quality control issues. This procedure gives a total of 557 stations, shown in Figure 8.

To compute the inverted barometer (IB) effect[33], we have used the ERA5 atmospheric reanalysis[37], which provides zonal and meridional winds and sea-level pressure. We computed the subsequent IB response using the standard relation from[33]. The zonal and meridional wind estimates used in the trajectory assessment are also from the ERA5 reanalysis. We sample the pressure and wind fields at the nearest ocean grid cell to each tide gauge.

To estimate the effects of large-scale teleconnection patterns on sea-level variability, we use the Multivariate ENSO index (MEI), the Pacific Decadal Oscillation index (PDO), and the North Atlantic Oscillation index (NAO). We computed annual-mean indices from the monthly indices from NOAA. The NAO, PDO, and MEI are often used as a proxy for large-scale unforced variability in sea level[38,39].

Barystatic processes, glacial isostatic adjustment, and vertical land motion

We estimate local sea-level changes and their uncertainties due to barystatic processes using the ensemble from[6]. This ensemble combines multiple in-situ estimates of barystatic sea-level changes before 2003, with observations from the GRACE and GRACE-Follow On gravimetry missions afterwards. From these barystatic estimates, regional sea-level variations due to GRD effects have been computed using the elastic sea-level equation solver as described in[6]. To assess sea-level observations from tide gauges corrected for VLM, we have to use the GSL GRD patterns. To obtain these GSL fields, we take the sum of the RSL and VLM fields. For this study, we have extended the record to 2019 using mass-change observations from the GRACE Follow-On satellite mission.

For GIA, we use the ensemble of estimates from[23]. This ensemble consists of sea-level and land-motion estimates that have been derived by perturbing ice histories and solid-earth properties and estimating the likelihood of each member by comparing

the solution to a wide array of observations. Here, we randomly select 100 members of this ensemble. We then compute local geocentric sea-level trends by adding up the RSL and VLM trends.

For our local VLM estimates, we use the GPS imaging estimates from the Nevada Geodetic Laboratory database[40].

Sterodynamic sea-level changes

Sterodynamic sea-level changes represent the combined effects of global thermosteric expansion and local ocean dynamics[32]. To estimate local sterodynamic sea-level variations, we separately estimate global thermosteric expansion and local ocean dynamics, following[12]. We obtain global thermosteric expansion from gridded observations of ocean subsurface temperatures. Following the procedure explained in[6], we use subsurface temperature estimates from three sources: the first is EN4 version 4.2.1[41]. The second dataset comes from[42], and the final estimate comes from[43]. From the subsurface temperature field, we compute density variations with respect to the product climatology using the TEOS-10 Gibbs Seawater equations[44]. These density variations are then translated into global-mean steric height variations. We take the mean of the three estimates (The EN4 estimate is the mean of each of the two XBT-bias-corrected estimates) to obtain annual-mean global-mean thermosteric variations. We do not consider global halosteric effects, which should be negligibly small on global scales[32].

For the dynamic part, we use the ECCO version 4 release 5 alpha ocean state estimate[45,46]. ECCO is an ocean state estimate, which uses the MITgcm ocean model, a wide array of observations, and an adjoint-based data assimilation approach to estimate a time-varying ocean state that strictly satisfies the physical constraints of the ocean model while being constrained by observations. ECCO version 4 release 5 has been run on a 1-degree horizontal resolution. From this state estimate, we use the dynamic sea-level fields, which represent sea-level variability due to ocean dynamics. For consistency with our definition of sterodynamic effects, we set the global-mean of the dynamic fields to zero. We then sample the dynamic field at the nearest ocean grid cell to the tide gauge, and add the global-mean thermosteric expansion.

Sea-level trajectories and projections

The sea-level trajectories we describe here are an estimate of the observed trend and acceleration at a specific tide-gauge location. We extrapolate this trend and acceleration forward to 2050 to assess future sea level rise if this trajectory is maintained over the coming decades. The presence of unforced sea-level variability has two important consequences for estimating the trajectory and its extrapolation:

1. The unforced variability affects the estimated trend and acceleration, which causes uncertainty in the extrapolated trajectory.

2. The future variability will lead to departures from this trajectory.

Together, these effects will create an envelope of possible sea-level changes about the estimated trajectory. Here, we account for both processes, and assess each effect separately.

To account for the first consequence, we first estimate the trend and acceleration from the tide-gauge record and its uncertainty. We use annual-mean tide-gauge observations over 1970-2020, which is a compromise between having a long record to robustly estimate the trend and acceleration and using a period where we can expect the long-term changes to be driven by forced changes. Since about 1970, global-mean sea level has persistently accelerated with a fairly constant rate[1] and this rise has been attributed to be largely a consequence of greenhouse gas forcings[47]. First, we estimate and remove some of the explainable unforced variability. We estimate the effects of zonal and meridional wind, surface pressure, and teleconnection patterns on local sea level using linear regression. We use time series of the three teleconnection patterns (NAO, PDO and MEI/Multivariate El Nino Index), and local pressure and wind stress anomalies from ERA5. We then compute the regression coefficient between these time series and observed sea level using ordinary least squares. We then multiply the time series with the regression coefficients and subtract them from the observations. This approach has been used in several previous studies[39,48], and assumes that these parameters are not affected by forced changes in the climate system. After removing these processes, we estimate the trend and acceleration from the time series. Since the regression model does not remove all sources of variability, the residual still contains serially-correlated variability. Therefore, we assume that the resulting time series can be described by a trend, acceleration, and first-order autoregressive process, which has been shown to be a suitable description of annual-mean sea level variability[49]. We estimate the autoregressive properties, the resulting trend and acceleration, and their uncertainties using the Hector software[34]. We then extrapolate the trajectory up to 2050. To assess the uncertainties, we generate a 5000-member ensemble of extrapolations, each of which has a perturbed trend and acceleration, based on their uncertainties. An example of this trajectory is shown in Figure 1: here, the blue line shows the annual-mean tide-gauge observations, the black line shows the estimated trajectory, and the shaded area the uncertainty (90% confidence interval) of the estimated trajectory, computed from the ensemble.

To account for the second consequence, we estimate the possible effects of unforced variability on the likely range of future sea-level change. To do this, we generate 5000 realizations of random noise with the same autoregressive properties

as observed sea level. Since this variability should account for the total expected variability, we generate the random noise using the autoregressive model properties of observed sea level without subtracting the estimated unforced variability. We then add the trajectories and the random variability to obtain an estimate of the likely range annual-mean of sea level up to 2050. The year 2050 has been chosen because on longer time scales, projections show a clear emissions-driven divergence[17], which implies that a simple extrapolation becomes less informative. The blue shading in Figure 1 shows this total range, which indicates the 90% confidence interval of present and future annual-mean sea level under the assumptions that the long-term changes are caught by the trajectory model and the unforced variability does not change. Figure 1 also shows a few individual trajectory realizations (colored thin lines).

From the ensemble we can compute many statistical properties, such as the expected change in sea level relative to the average over 2001-2020 for various years. Some are shown in the right panel of Figure 1. In this example, the expected sea-level change in 2025, relative to the 2001-2020 mean, is about 5 cm, but due to the uncertainties in the trajectory and the presence of unforced variability, the likely total range will be between 0 and 10 cm. Hence, due to unforced variability, zero observed sea-level change in 2025 relative to the 2001-2020 mean is still within the likely range when sea level keeps following the present trajectory. On the other hand, a rise of 10 cm in 2025 also does not imply sea level has changed its trajectory. The further ahead in time, the uncertainties become larger, and the uncertainties in the trajectory become the largest contributor to the total variability.

References

1. Dangendorf, S. *et al.* Persistent acceleration in global sea-level rise since the 1960s. *Nat. Clim. Chang.* DOI: 10.1038/s41558-019-0531-8 (2019).
2. Slangen, A. B. A., van de Wal, R. S. W., Wada, Y. & Vermeersen, L. L. A. Comparing tide gauge observations to regional patterns of sea-level change (1961-2003). *Earth Syst. Dyn.* **5**, 243–255, DOI: 10.5194/esd-5-243-2014 (2014).
3. Nicholls, R. Planning for the Impacts of Sea Level Rise. *Oceanography* **24**, 144–157, DOI: 10.5670/oceanog.2011.34 (2011).
4. Haigh, I. D. *et al.* Timescales for detecting a significant acceleration in sea level rise. *Nat. Commun.* **5**, DOI: 10.1038/ncomms4635 (2014).
5. Fasullo, J. T. & Nerem, R. S. Altimeter-era emergence of the patterns of forced sea-level rise in climate models and implications for the future. *Proc. Natl. Acad. Sci.* 201813233, DOI: 10.1073/pnas.1813233115 (2018).
6. Frederikse, T. *et al.* The causes of sea-level rise since 1900. *Nature* **584**, 393–397, DOI: 10.1038/s41586-020-2591-3 (2020).
7. Royston, S. *et al.* Can We Resolve the Basin-Scale Sea Level Trend Budget From GRACE Ocean Mass? *J. Geophys. Res. Ocean.* **125**, DOI: 10.1029/2019JC015535 (2020).
8. Shirzaei, M. *et al.* Measuring, modelling and projecting coastal land subsidence. *Nat. Rev. Earth & Environ.* **2**, 40–58, DOI: 10.1038/s43017-020-00115-x (2021).
9. Dangendorf, S. *et al.* Data-driven reconstruction reveals large-scale ocean circulation control on coastal sea level. *Nat. Clim. Chang.* DOI: 10.1038/s41558-021-01046-1 (2021).
10. Piecuch, C. G. *et al.* Origin of spatial variation in US East Coast sea-level trends during 1900–2017. *Nature* **564**, 400–404, DOI: 10.1038/s41586-018-0787-6 (2018).
11. Frederikse, T. *et al.* Closing the sea level budget on a regional scale: Trends and variability on the Northwestern European continental shelf. *Geophys. Res. Lett.* **43**, 10,864–10,872, DOI: 10.1002/2016GL070750 (2016).
12. Harvey, T. C. *et al.* Ocean mass, sterodynamic effects, and vertical land motion largely explain US coast relative sea level rise. *Commun. Earth & Environ.* **2**, 233, DOI: 10.1038/s43247-021-00300-w (2021).
13. Wang, J. *et al.* Evaluation of the local sea-level budget at tide gauges since 1958. *Geophys. Res. Lett.* DOI: 10.1029/2021GL094502 (2021).
14. Church, J. *et al.* Sea Level Change. In Stocker, T. *et al.* (eds.) *Climate Change 2013: The Physical Science Basis. Contribution of Working Group I to the Fifth Assessment Report of the Intergovernmental Panel on Climate Change*, book section 13, 1137–1216, DOI: 10.1017/CBO9781107415324.026 (Cambridge University Press, Cambridge, United Kingdom and New York, NY, USA, 2013).
15. Wang, J., Church, J. A., Zhang, X. & Chen, X. Reconciling global mean and regional sea level change in projections and observations. *Nat. Commun.* **12**, 990, DOI: 10.1038/s41467-021-21265-6 (2021).

16. Dangendorf, S. *et al.* Evidence for long-term memory in sea level. *Geophys. Res. Lett.* **41**, 5530–5537, DOI: 10.1002/2014GL060538 (2014).

17. Fox-Kemper, B. & Hewitt, H. Ocean, Cryosphere and Sea Level Change. In Masson-Delmotte, V. (ed.) *Climate Change 2021: The Physical Science Basis. Contribution of Working Group I to the Sixth Assessment Report of the Intergovernmental Panel on Climate Change* (Cambridge University Press, 2021).

18. Garner, G. *et al.* IPCC AR6 Sea-Level Rise Projections (2021).

19. Forget, G. & Ponte, R. M. The partition of regional sea level variability. *Prog. Oceanogr.* **137**, 173–195, DOI: 10.1016/j.pocean.2015.06.002 (2015).

20. Hamlington, B. D. *et al.* The Dominant Global Modes of Recent Internal Sea Level Variability. *J. Geophys. Res. Ocean.* **124**, 2750–2768, DOI: 10.1029/2018JC014635 (2019).

21. Hamlington, B. *et al.* Past, Present and Future Pacific Sea Level-Change. *Earth's Futur.* DOI: 10.1029/2020EF001839 (2020).

22. Calafat, F. M., Chambers, D. P. & Tsimplis, M. N. Mechanisms of decadal sea level variability in the eastern North Atlantic and the Mediterranean Sea. *J. Geophys. Res. Ocean.* **117**, DOI: 10.1029/2012JC008285 (2012).

23. Caron, L. *et al.* GIA Model Statistics for GRACE Hydrology, Cryosphere, and Ocean Science. *Geophys. Res. Lett.* **45**, 2203–2212, DOI: 10.1002/2017GL076644 (2018).

24. Larsen, C. F., Motyka, R. J., Freymueller, J. T., Echelmeyer, K. A. & Ivins, E. R. Rapid uplift of southern Alaska caused by recent ice loss: Rapid uplift of southern Alaska. *Geophys. J. Int.* **158**, 1118–1133, DOI: 10.1111/j.1365-246X.2004.02356.x (2004).

25. Riddell, A. R., King, M. A. & Watson, C. S. Present-Day Vertical Land Motion of Australia From GPS Observations and Geophysical Models. *J. Geophys. Res. Solid Earth* **125**, DOI: 10.1029/2019JB018034 (2020).

26. Kolker, A. S., Allison, M. A. & Hameed, S. An evaluation of subsidence rates and sea-level variability in the northern Gulf of Mexico. *Geophys. Res. Lett.* **38**, n/a–n/a, DOI: 10.1029/2011GL049458 (2011).

27. Karegar, M. A., Dixon, T. H. & Engelhart, S. E. Subsidence along the Atlantic Coast of North America: Insights from GPS and late Holocene relative sea level data. *Geophys. Res. Lett.* **43**, 3126–3133, DOI: 10.1002/2016GL068015 (2016).

28. Kopp, R. E. Does the mid-Atlantic United States sea level acceleration hot spot reflect ocean dynamic variability? *Geophys. Res. Lett.* **40**, 3981–3985, DOI: 10.1002/grl.50781 (2013).

29. Little, C. M. *et al.* The Relationship Between U.S. East Coast Sea Level and the Atlantic Meridional Overturning Circulation: A Review. *J. Geophys. Res. Ocean.* 2019JC015152, DOI: 10.1029/2019JC015152 (2019).

30. Woodworth, P., Wöppelmann, G., Marcos, M., Gravelle, M. & Bingley, R. Why We Must Tie Satellite Positioning to Tide Gauge Data. *Eos* DOI: 10.1029/2017EO064037 (2017).

31. Hausfather, Z. & Peters, G. P. Emissions – the 'business as usual' story is misleading. *Nature* **577**, 618–620, DOI: 10.1038/d41586-020-00177-3 (2020).

32. Gregory, J. M. *et al.* Concepts and Terminology for Sea Level: Mean, Variability and Change, Both Local and Global. *Surv. Geophys.* DOI: 10.1007/s10712-019-09525-z (2019).

33. Wunsch, C. & Stammer, D. Atmospheric loading and the oceanic "inverted barometer" effect. *Rev. Geophys.* **35**, 79–107, DOI: 10.1029/96RG03037 (1997).

34. Bos, M. S., Fernandes, R. M. S., Williams, S. D. P. & Bastos, L. Fast error analysis of continuous GNSS observations with missing data. *J. Geod.* **87**, 351–360, DOI: 10.1007/s00190-012-0605-0 (2013).

35. Holgate, S. J. *et al.* New Data Systems and Products at the Permanent Service for Mean Sea Level. *J. Coast. Res.* **288**, 493–504, DOI: 10.2112/JCOASTRES-D-12-00175.1 (2013).

36. PSMSL. Permanent Service for Mean Sea Level, tide gauge data retrieved on 1 Nov 2021 from http://www.psmsl.org/data/obtaining/ (2021).

37. Hersbach, H. *et al.* The ERA5 global reanalysis. *Q. J. Royal Meteorol. Soc.* **146**, 1999–2049, DOI: 10.1002/qj.3803 (2020).

38. Zhang, X. & Church, J. A. Sea level trends, interannual and decadal variability in the Pacific Ocean. *Geophys. Res. Lett.* **39**, n/a–n/a, DOI: 10.1029/2012GL053240 (2012).

39. Calafat, F. M. & Chambers, D. P. Quantifying recent acceleration in sea level unrelated to internal climate variability. *Geophys. Res. Lett.* **40**, 3661–3666, DOI: 10.1002/grl.50731 (2013).

40. Hammond, W. C., Blewitt, G., Kreemer, C. & Nerem, R. S. GPS Imaging of Global Vertical Land Motion for Studies of Sea Level Rise. *J. Geophys. Res. Solid Earth* **126**, DOI: 10.1029/2021JB022355 (2021).

41. Good, S. A., Martin, M. J. & Rayner, N. A. EN4: Quality controlled ocean temperature and salinity profiles and monthly objective analyses with uncertainty estimates. *J. Geophys. Res. Ocean.* **118**, 6704–6716, DOI: 10.1002/2013JC009067 (2013).

42. Cheng, L. & Zhu, J. Benefits of CMIP5 Multimodel Ensemble in Reconstructing Historical Ocean Subsurface Temperature Variations. *J. Clim.* **29**, 5393–5416, DOI: 10.1175/JCLI-D-15-0730.1 (2016).

43. Ishii, M. *et al.* Accuracy of Global Upper Ocean Heat Content Estimation Expected from Present Observational Data Sets. *SOLA* **13**, 163–167, DOI: 10.2151/sola.2017-030 (2017).

44. McDougall, T. J. & Barker, P. M. *Getting Started with TEOS-10 and the Gibbs Seawater (GSW) Oceanographic Toolbox* (Trevor J McDougall, Battery Point, Tas., 2011).

45. Forget, G. *et al.* ECCO version 4: An integrated framework for non-linear inverse modeling and global ocean state estimation. *Geosci. Model. Dev.* **8**, 3071–3104, DOI: 10.5194/gmd-8-3071-2015 (2015).

46. ECCO Consortium *et al.* Synopsis of the ECCO Central Production Global Ocean and Sea-Ice State Estimate, Version 4 Release 4. Tech. Rep., Zenodo (2021). DOI: 10.5281/ZENODO.4533349.

47. Slangen, A. B. A. *et al.* Anthropogenic forcing dominates global mean sea-level rise since 1970. *Nat. Clim. Chang.* **6**, 701–705, DOI: 10.1038/nclimate2991 (2016).

48. Frederikse, T. & Gerkema, T. Multi-decadal variability in seasonal mean sea level along the North Sea coast. *Ocean. Sci.* **14**, 1491–1501, DOI: 10.5194/os-14-1491-2018 (2018).

49. Royston, S. *et al.* Sea-Level Trend Uncertainty With Pacific Climatic Variability and Temporally-Correlated Noise. *J. Geophys. Res. Ocean.* **123**, 1978–1993, DOI: 10.1002/2017JC013655 (2018).

Acknowledgements

Parts of this work were carried out in part at the Jet Propulsion Laboratory, California Institute of Technology, under a contract with the National Aeronautics and Space Administration (80NM0018D0004).

Author contributions statement

TF and BH conceived the idea of this study. TF conducted all computations with support of CH, TF wrote the manuscript and compiled the figures. IFe, OW, and IFu provided the ECCO datasets. BH, CH, WS, OW, and IFu assisted in writing the manuscript.

Competing interests

The authors declare no competing interests.

Data availability

All scripts and data will be placed in a permanent repository (Zenodo) upon acceptance of the final version. A zip file with all scripts, results, and one-pagers per location can be downloaded from `https://thomasfrederikse.stackstorage.com/s/pDvIUjfnV76Hnfiu`